Acoustic and thermal performance of polypropylene nonwoven fabrics for insulation in buildings

Faezeh Karimi[1], Parham Soltani[1*], Mohammad Zarrebini[1], Ali Hassanpour[2]

[1] *Department of Textile Engineering, Isfahan University of Technology, Isfahan 84156-83111, Iran*

[2] *School of Chemical and Process Engineering, University of Leeds, LS2 9JT Leeds, UK*

Abstract

Thermal insulation and acoustic absorption materials play a significant role in the characteristics of energy-saving and comfortable modern buildings. However, these two types of materials are generally developed independently. This study highlights the potential of lightweight polypropylene nonwoven fabrics for building applications and investigates how fabric structure affects thermal and acoustical properties. An industrial-scale melt spinning machine was used to produce polypropylene fibers at linear densities of 1.4 and 1.8 dtex. A semi-industrial needle punching line was used to fabricate nonwoven samples with three thicknesses (2, 3, and 4 cm), four porosities (0.83, 0.88, 0.93, and 0.96), and different in- and through-plane fiber orientation distributions. Totally, 31 samples were produced and their sound absorption and thermal insulation performance were assessed using impedance tube and guarded hot plate techniques. Accordingly, the thermal conductivity (K_{eff}) and sound absorption average (SAA) of the samples could be engineered in the range of 0.0270-0.0404 W.m^{-1}K^{-1} and 0.270–0.675, respectively. It was found that fabrics made of finer fibers provide superior acoustic absorption and thermal insulation performance. An increase in through-plane fiber orientation adversely affected the thermal insulation properties, while its effect on acoustic properties depends on the porosity of

---

[*] E-mail addresses: pa.soltani@iut.ac.ir
Tel.: +98 3133911093; fax: +98 3133912441

samples and the sound frequency. The results of statistical analysis showed that in-plane fiber orientation does not have a significant effect on sound absorption behavior, except at frequencies between 4000-6300 Hz. It was also found that in-plane fiber orientation does not significantly affect the thermal insulation properties. The best acoustic and thermal performance were achieved by fibrous samples of layered structure made of 1.4 dtex fibers with a thickness of 3 cm (K_{eff}=0.0278 W.m^{-1}K^{-1}, SAA= 0.552) and 4 cm (K_{eff}=0.0277 W.m^{-1}K^{-1}, SAA= 0.675). The performance of these samples was compared with some commercial products and literature data. The results pointed to the superior acoustic and thermal properties of the designed samples.

Keywords: Polypropylene nonwoven; acoustic properties; thermal insulation; 3D fiber orientation; porosity; fabric structure

1. Introduction

The rapid economic development and increasing anthropogenic activities in recent years have given rise to environmental issues such as global warming and noise pollution. In the face of the depletion of natural energy resources and the increase of greenhouse gases, the policies and strategies of the majority of world countries are aimed at the reduction of energy consumption in sectors with the highest energy intensity. Residential and commercial buildings accounted for almost 41% of global energy consumption [1, 2], approximately 40-50% of the greenhouse gas emissions [3], and about 33% of CO_2 productions [4]. Therefore, buildings might be considered as one of the most important sectors for potential improvement. Insulation in buildings leads to the reduction of energy consumption by minimizing the gains and losses of heat during the cooling and heating of the building. Hadded et al. [5] reported that appropriate insulation could reduce energy consumption by approximately 70% in residential buildings. Generally, the thermal insulating materials are categorized as (i) conventional (e.g., fibrous [6],

fiber-reinforced composites [7], and foam media [8]), (ii) state-of-the-art (e.g., silica aerogels [9] and vacuum insulation panels [10]), and (iii) possible future thermal insulation media (e.g., load-bearing [11] and gas insulating media [12]). Currently, the two latter categories are under research and development and have not reached the stage of practical applications in building. They also suffer from sophisticated preparation and fabrication processes, high cost, and low mechanical properties [13, 14]. The conventional thermal insulating media based on their composition are categorized as organic [15-17] and inorganic [18-20]. Although inorganic insulating materials are low-cost, durable and incombustible, however, their apparent density is generally high. Moreover, their manufacturing process requires very high temperature and also results in a massive amount of carbon emission, therefore, they cannot meet the energy-saving requirements of modern buildings [21]. Thermal insulation characteristics of synthetic organic polymers such as polyester (PET) and polypropylene (PP) are generally not as good as inorganic ones [22]. However, they are generally preferred thermal insulation materials because of their stable physical and chemical characteristics, low apparent density, and production cost, which render them particularly suitable for building applications [23].

PP, once discovered, immediately found a wide range of applications because of its remarkable and miscellaneous characteristics such as excellent chemical and corrosion resistance, low moisture absorption, good recyclability, and easy processability. Additionally, PP has the lowest density (i.e., 0.91 g/cm^3) among the thermoplastic polymers, which results in a very low cost per unit volume, giving PP a further advantage over other fibers [24].

Several investigations have been carried out on the thermal insulation properties of nonwoven fibrous structures. These studies have shown that various parameters such as

3

fiber diameter distribution (FDD), fiber orientation distribution (FOD), pore size distribution (PSD), fabric density, and thickness affect the thermal resistance of the nonwoven fabrics [25-31].

On the other hand, in recent years, noise pollution has become more prominent and pervasive due to population growth, urbanization, and industrialization in the cities. Noise pollution has substantial negative consequences on human health [32-34]. Therefore, strict legislation around the world has been introduced concerning the control of noise pollution. Nonwoven fabrics, due to their complex irregular porous structure, high surface area, the ability to engineer their micro-structure, and low cost, are ideal materials for sound absorption applications. A wealth of experimental investigations have been conducted on the acoustic behavior of nonwoven fabrics made of natural and synthetic fibers. These studies have shown that fabric thickness and porosity significantly affect the sound absorption characteristics of these structures [35-41]. The investigations on the effect of fabric microstructure such as FOD and PSD on the acoustic absorption behavior of nonwovens have been focused on theoretical [42-45] and numerical [46-48] studies. The scarcity of experimental studies in this field is related to the fact that investigation of microstructure effect on acoustic behavior requires substantial experimental data, which is both time-consuming and costly. Moreover, non-destructive 3D imaging techniques that enable accurate characterization of the internal microstructure of porous media such as pore size and 3D fiber orientation have recently been developed.

A solution to achieve the highest possible thermal insulation and sound absorption in buildings is to increase the thickness of nonwoven insulation or absorber installed in the building envelope. However, very thick building envelopes are not desirable due to architectural restrictions, indoor floor space reductions, material usage, and other

limitations. In order to produce nonwoven fibrous media with efficient thermal resistance and sound absorption while keeping the thickness as low as possible, the structure of the media must be engineered. Structural parameters such as PSD, FDD, FOD, and porosity affect the thermal and acoustical characteristics of nonwoven fabrics. To the best of our knowledge, there has been no reported investigation on the experimental evaluation of these parameters for both thermal insulation and acoustic absorption properties. To this end, in this study, polypropylene nonwovens with different structural properties are produced using a semi-industrial batt forming-needling line. Thermal insulation and sound absorption behavior of the samples are assessed using the guarded hot plate and two-microphone impedance tube, respectively. Additionally, the structural parameters of the samples are characterized using X-ray micro-computed tomography (μCT). Finally, the effect of structural properties on thermal insulation and acoustic absorption performance of the samples is investigated.

2. Experimental

2.1 Fiber production

PP granules (Moplen X30S: MFI at 230°C=25 g/10min, density of 910 Kg/m^3, and molecular weight of 150 kg/mol) were supplied by Maroon Petrochemical Company (Mahshahr, Iran). PP fibers were spun on an industrial-scale melt spinning machine. Under constant pressure, the polymer melt was fed to spinnerets after passing through spinning pumps. The emerged filaments from spinnerets were quenched using a cold water bath. The spun filaments suffer from inadequate mechanical properties. These inadequacies can be significantly improved by feeding the filament tows to a number of drawing stations known as godets where the filaments under tensile force are elongated and thus the degree of crystallization of the molecular structure of the filaments are

greatly enhanced. The PP granules were melted in an extruder having an L:D of 30. A temperature profile of 170℃ to 210℃ was used along the length of the extruder under the constant pressure of 135 bar. Fiber fineness was adjusted by manipulation of spinning pump speed and variation in the chosen draw ratio. PP filaments with linear densities of 1.4 and 1.8 dtex were produced and cut into 90 ± 3 mm staple fibers using a Lummas type cutter. Fig. 1 shows the schematic of fiber production.
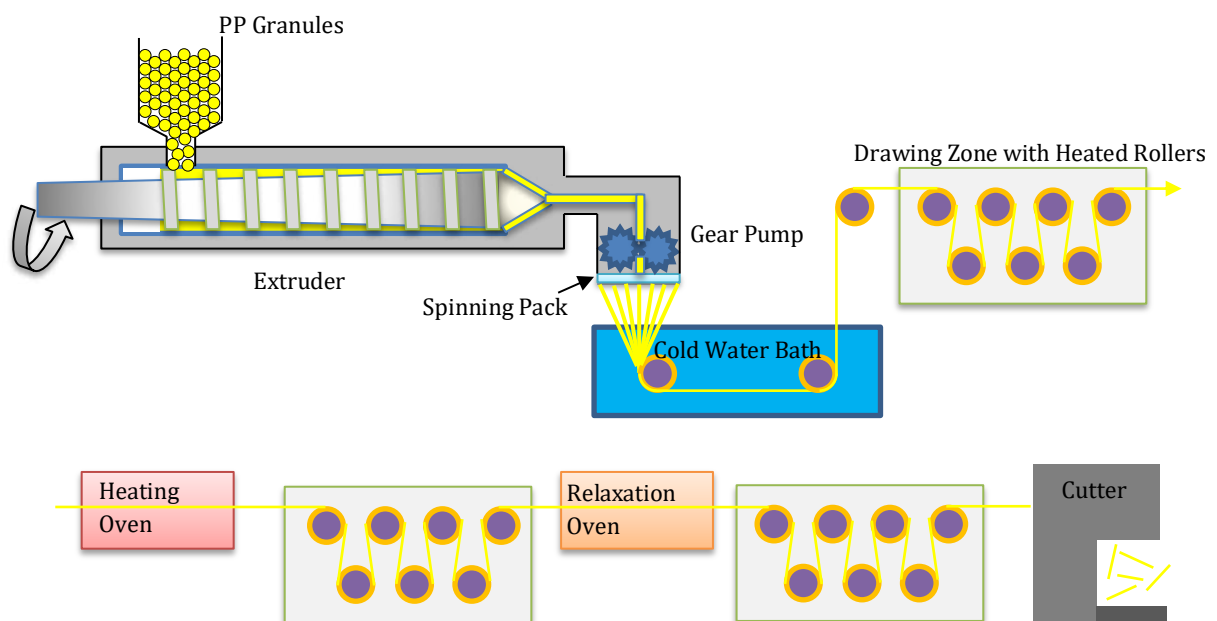
Fig. 1 Schematic of industrial-scale melt spinning machine

2.2 Sample preparation

In this study, the acoustic and thermal properties of PP needled nonwoven fabrics were investigated. These easy-to-manufacture and cost-effective fabrics have gained considerable importance over the past years in the field of sound absorption and thermal insulation thanks to the capability of engineering the microstructure.

A semi-industrial scale needling line comprised of a pair of feed rollers, carding machine, cross-folder, and needling loom was employed to make the required samples. To fabricate these specimens, the conditions of the cross-lapping and needling process were controlled to produce systematic variations in porosity, thickness, and in-plane (IP) and through-plane (TP) fiber orientation. Almost individualized fibers were fed to the carding machine to produce carded webs. The resultant more or less parallel-oriented fibrous webs were then introduced to the cross-folding machine to transform into fibrous batts. The IP fiber orientation in the cross-folded batt is perpendicular to the initial fiber orientation in the carded web. The batt fiber orientation can be altered by varying the ratio of liner speed of the input web into the cross-folder and the output batt. The number of fibrous webs in the layered batt controls the weight and the thickness of the resultant batts. The desirable batts, as far as IP fiber orientation, weight, and thickness were concerned, were fed to the needling loom. Mechanical entanglement of the batt was achieved due to repeated interlocking of the fibers of the batts with an array of special barbed needles. During penetration of the batt by the barbed needles, changes in the TP orientation of the batt take place, which in turn results in the changes in thickness, density, and porosity of the needled batt. Production parameters were adjusted so that needled nonwoven fabric specimens at 25, 55, 85, 115, and 135 punches per square centimeter were prepared. The needling operation was carried out at needle penetration depths of 8 and 11 mm. Specimens were produced at a temperature of 22±2°C and RH of 63 ± 2% using Groz-Beckert barbed needles. The properties of samples are given in Table 1. Some images of the samples are also illustrated in Fig. 2.

Table 1 Characteristics of the samples *

Sample code	T (cm)	F (dtex)	σ (Nm⁻⁴s)	ρ (%)	3D fiber orientation			K_{eff} (W.m⁻¹K⁻¹)	R (m² K/W)
					a_{11}	a_{22}	a_{33}		
1	2	1.4	85137	0.832	0.33	0.31	0.36	0.0353	0.5666
2	2	1.4	71021	0.884	0.30	0.34	0.36	0.0315	0.6349
3	2	1.4	49800	0.933	0.32	0.30	0.38	0.0299	0.6689
4	2	1.4	19055	0.966	0.32	0.33	0.35	0.0274	0.7299
5	2	1.8	72019	0.827	0.34	0.31	0.35	0.0376	0.5319
6	2	1.8	60020	0.887	0.33	0.30	0.37	0.0343	0.5831
7	2	1.8	38100	0.935	0.30	0.34	0.36	0.0319	0.6270
8	2	1.8	14022	0.968	0.34	0.31	0.35	0.0297	0.6734
9	3	1.4	88880	0.824	0.29	0.35	0.36	0.0347	0.8645
10	3	1.4	75050	0.877	0.35	0.32	0.33	0.0328	0.9146
11	3	1.4	52211	0.926	0.35	0.33	0.34	0.0301	0.9966
12	3	1.4	24100	0.961	0.33	0.33	0.33	0.0278	1.0791
13	3	1.8	66011	0.833	0.34	0.30	0.36	0.0372	0.8064
14	3	1.8	54112	0.874	0.31	0.32	0.37	0.0349	0.8596
15	3	1.8	33290	0.934	0.33	0.32	0.35	0.0317	0.9464
16	3	1.8	10917	0.954	0.30	0.33	0.37	0.0309	0.9709
17	4	1.4	91965	0.829	0.29	0.34	0.37	0.0357	1.1204
18	4	1.4	76825	0.878	0.32	0.32	0.36	0.0330	1.2121
19	4	1.4	58586	0.926	0.33	0.30	0.37	0.0303	1.3201
20	4	1.4	27655	0.966	0.34	0.32	0.34	0.0277	1.4440
21	2	1.4	90216	0.830	0.42	0.45	0.13	0.0328	0.6097
22	2	1.4	78073	0.834	0.24	0.26	0.50	0.0369	0.5420
23	2	1.4	70065	0.827	0.14	0.15	0.71	0.0404	0.5038
24	2	1.4	55563	0.928	0.46	0.43	0.11	0.0285	0.7017
25	2	1.4	40145	0.926	0.25	0.23	0.52	0.0309	0.6472
26	2	1.4	30884	0.932	0.17	0.15	0.68	0.0323	0.6192
27	2	1.4	29656	0.964	0.44	0.41	0.15	0.0270	0.7407
28	2	1.4	12061	0.960	0.23	0.24	0.53	0.0281	0.7117
29	2	1.4	10006	0.959	0.14	0.14	0.72	0.0290	0.6896
30	2	1.4	53934	0.932	0.59	0.31	0.10	0.0281	0.7117
31	2	1.4	49821	0.927	0.72	0.16	0.12	0.0292	0.6849

* T= Thickness, F= Fiber linear density, σ= Flow resistivity, ρ= Porosity, K_{eff} = Effective thermal conductivity, and R= Thermal resistance

Sample 1	Sample 9
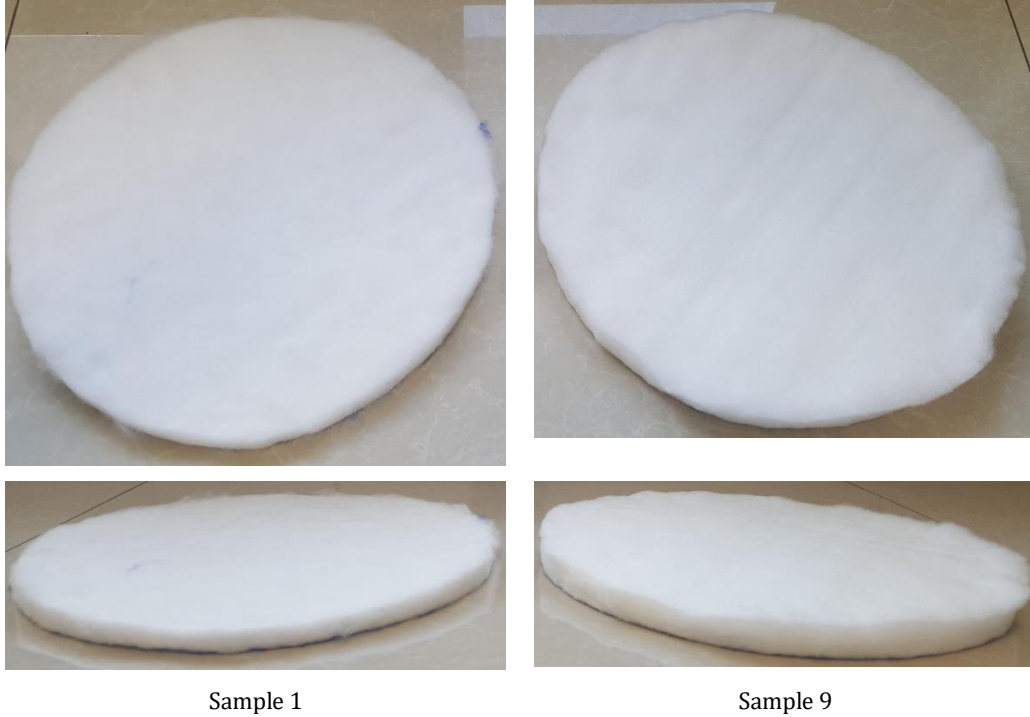
Fig. 2 Some images of the samples

2.3 Physical parameters measurement

Prior to tests, samples were conditioned for 24 h at RH and temperature of 63±2% and 23°C, respectively. The linear density of fibers (F) was determined using Vibroskop 400 (Lenzing Technik, Austria) following the ASTM D1577. The thickness (T) of the samples was measured according to ASTM D5729-97, using a thickness tester (Shirley Developments Ltd, Manchester) at different locations on the samples. The measurements were performed at least eight times, and the average was calculated. The areal density was measured according to BS 12127 using a digital balance (Shimadzu, model UX2200H, Japan). The measurements were performed three times, and the average was calculated. The solid volume fraction of samples (φ) was calculated using Eq. 1:

$$\varphi = \frac{Fabric\ density}{Fiber\ density} \tag{1}$$

The density of PP was considered to be 0.91 g/cm^3.

2.4 Airflow resistivity

KES-F80-AP1 instrument (Kato Tech Co., Ltd., Japan) was used to measure the resistance to air. Circular specimens of 50 cm^2 were cut from each sample. Five specimens from each fibrous network were tested, and the mean was reported.

2.5 Sound absorption

Sound absorption characteristics of the samples were assessed according to ASTM E1050, using an impedance tube (SW477, BSWA Technology Co., Ltd.). The tests were conducted at an RH of 60±2% and a temperature of 23°C.

A signal generator that is used to generate broadband, stationary random sound waves drives a loudspeaker through a power amplifier. The threshold frequency of sound waves depends on the internal diameter of the impedance tube. The tubes of 30 mm and 100 mm diameter were respectively used for the measurement of sound absorption coefficient (SAC) at frequency bands of 1600-6300 Hz and 80-1600 Hz. The loudspeaker propagates plane acoustic waves in the tube. The acoustic waves strike the test specimen installed at the end of the tube and are backed with a rigid plate. As a result of the superposition of the forward- and backward-traveling acoustic waves, a standing-wave interference pattern is generated. Two microphones are placed flush to the inner wall of the tube at a certain separation distance and measure the sound pressure. The transfer function technique [49] was employed to measure the SAC of the samples. In this method, the incident and reflected sound pressure from the measured complex transfer function between the microphones are separated, and the SAC is calculated. The measurements for each sample were performed three times, and the average was calculated.

The sound absorption average (SAA) of the samples was also calculated as defined by ASTM C423-09A. It is the arithmetic average value of twelve 1/3 octave band SACs at frequencies ranging from 200 to 2500 Hz.

2.6 Thermal conductivity and thermal resistance

Generally, the effective thermal conductivity (K_{eff}) and thermal resistance (R), which include the contributions of the fibers and the air, are used to assess the overall performance of fibrous insulation media. The thermal resistance (R) values of the specimens were assessed according to ISO 5085, using the guarded hot plate apparatus. The apparatus works based on one-dimensional Fourier's law. According to this law, the ratio of temperature drop across the conductors connected in series with respect to the heat flow direction is equal to the ratio of their thermal resistance. Therefore, the thermal resistance of a specimen can be measured if it is arranged in series with a "reference resistance" of known thermal resistance. The setup is enclosed in a cabinet to provide a shield against other sources of radiant heat and achieve controlled ventilation across the face of the apparatus. Thermal resistance measurements were taken using 330 mm circular specimens. The measurements were carried out at an RH of 60±2%. Measurements for each sample were performed three times, and the average was calculated.

For a nonwoven insulation medium, K_{eff} is affected by the porosity of medium, fiber fineness, 3D fiber orientation, and fibers and air thermal conductivity. Thermal resistance is related to the thickness of the medium (T) and is calculated as follows:

$$R = \frac{T}{K_{eff}}$$

(2)

The K_{eff} and R values of samples are given in Table 1.

2.7 μCT visualization

μCT is a non-destructive imaging method that allows three-dimensional (3D) visualization of the internal structure of materials such as fibrous porous media. A Phoenix Nanotom μCT (GE Sensing & Inspection, Germany), equipped with a nano focus tube was used to scan the 3D microstructure of samples. Specimens were cut from the samples using a diamond blade and placed on the rotation stage between the X-ray source and a series of 2048×2048 pixels flat-panel detectors. A total of 2200 projection images per scan were taken with 0.1 ° projection intervals for a full angular range of 0-360 °. To enhance the signal-to-noise ratio, each projection was obtained by averaging three 2D X-ray images. The range of settings for scanning was: acceleration voltage of 100-130 kV, emission current of 110-120 μA, exposure time of 600 ms for each image, and an isotropic voxel size of 3.1-3.3 μm on the specimen dimensions.

2.7.1 *Data processing*

The volumes were reconstructed with Datos|x 2.0 (General Electric Sensing and Inspection Technologies, Wunstorf, Germany) by an ultra-high-resolution noise-reducing filter back-projection algorithm. The reconstructed image contains a stack of 2D cross-section images of the specimen with an 8-bit gray value distribution. For an 8-bit image, the intensity value varies from 0 to 255. In order to reduce random noise, these images were twice Gaussian filtered (3×3×3). The gray values in the rendered μCT images indicate the attenuation in each voxel. The lower density phase (i.e., air) appears darker as compared with the higher density phase (i.e., fiber).

For further analysis, the 2D cross-sectional images were imported into the Avizo® software and rendered into a 3D image. Several mathematical morphological operations,

including erosion, dilation, and filling gaps, were applied to the X-ray images. Afterward, segmentation of the image was performed using the *Triangle* Method developed by Zack et al. [50]. Segmentation is the process of converting the gray-scale image into a binarized image of the solid and void phases. Fig. 3 shows an example of a reconstructed image.

Fig. 3 A typical 3D rendered image of nonwoven fabric

2.7.2 *Morphological analysis*

Morphological characterization of samples was performed using image analysis techniques using an in-house code developed by Matlab and the Avizo® software.

Porosity

Once the binarized 3D volume is obtained, the solid volume fraction (SVF) can be calculated as the ratio of voxels assigned to the fibrous phase to the total number of voxels in the 3D volume. The porosity was then calculated as 1-SVF.

Spatial fiber orientation

In order to measure the 3D FOD in the fibrous network, a code was developed in Matlab. To this end, the reconstructed segmented fibers were first thinned to their medial axes. The medial axes, also called skeletons, are essentially a network of one-dimensional paths and nodes at path intersections, which topologically are identical to that of the fibrous network. The code uses the skeletonization algorithm proposed by Viguié et al. [51], which is based on distance-map and watershed. When two fibers are crossing at an acute angle, their medial axis appears as ladder-shaped and contains a substantial number of spurious paths. These paths were eliminated by the "surface remnant reduction algorithm" proposed by the authors [52].

Once the 3D skeletonized network structure was obtained, the direct-tracing algorithm proposed by the authors [53] was used to calculate the spatial fiber orientation. The orientation of fibers in 3D space was expressed by the second-order tensor a as follows:

$$a = \frac{1}{l_{tot}} \sum l_i \begin{bmatrix} \sin^2 \theta_i \cos^2 \varphi_i & \sin^2 \theta_i \sin \varphi_i \cos \varphi_i & \cos \theta_i \sin \theta_i \cos \varphi_i \\ \sin^2 \theta_i \sin \varphi_i \cos \varphi_i & \sin^2 \theta_i \sin^2 \varphi_i & \cos \theta_i \sin \theta_i \cos \varphi_i \\ \cos \theta_i \sin \theta_i \cos \varphi_i & \cos \theta_i \sin \theta_i \cos \varphi_i & \cos^2 \theta_i \end{bmatrix} \quad (3)$$

where l_i is the ith fiber segment length, l_{tot} denotes the total fiber length in the 3D volume, $0 \leq \theta_i \leq \pi$ represents the angle between the ith fiber segment axis and the z-axis, $0 \leq \varphi_i \leq 2\pi$ denotes the angle between the projection of the ith fiber segment on the $x - y$ plane and the x-axis.

The diagonal components of a_{ij} must always lie in the range [0, 1]. The tensor a is symmetric, and its trace always equals one, i.e., $a_{11} + a_{22} + a_{33} = 1$. The diagonal components serve to characterize the relative orientation in x-, y- and z-directions. Therefore, in an isotropic fibrous structure $a_{11} = a_{22} = a_{33} = 1/3$, and in a layered structure $a_{11} = a_{22} = 1/2$, and a_{33}=0.

3. Results and discussions

In this study, 31 samples were produced using different production parameters which have resulted in different physical and structural characteristics in terms of thickness (2, 3, and 4 cm), porosity (0.83, 0.88, 0.93, and 0.96), 3D fiber orientation (in-plane and through-plane), and linear density of fibers (1.4 and 1.8 dtex), as shown in Table 1.

The spatial orientation of fibers in samples 1-20 is isotropic. Samples 1-4 were produced at a thickness of 2 cm, and fiber linear density of 1.4 dtex at four different porosity values to investigate the effect of porosity on acoustic and thermal properties. In order to study the effect of porosity on the properties of samples made of 1.8 dtex fibers, samples 5-8 were produced at a thickness of 2 cm and four different porosity values. Samples 9-12 and 13-16 were manufactured from fibers of 1.4 and 1.8 dtex, respectively at four different porosity values to investigate the effect of fiber linear density and porosity at a thickness of 3 cm. Samples 17-20 were produced at a thickness of 4 cm, fiber linear density of 1.4 dtex, and four different porosity values. Comparison of samples 1-20 shows the simultaneous effects of sample thickness, fiber linear density, and porosity for the samples of isotropic fiber orientation. Sample 21-23 were produced at a thickness of 2 cm, fiber linear density of 1.4 dtex, and porosity of 0.83 at different through-plane fiber orientation distributions. Samples 24-26 and 27-29 had the same structural parameter as those of samples 21-23 with the difference that their porosity was 0.93 and 0.96, respectively. Samples 24, 30, and 31 were fabricated at a thickness of 2 cm, fiber linear density of 1.4 dtex, porosity of 0.93, and different in-plane fiber orientation distributions.

The effects of these parameters on the sound absorption properties and thermal resistance characteristics are discussed in the following sections.

3.1 Flow resistivity

Fig. 4a shows the variations of flow resistivity values for samples 1-8. As is observed, flow resistivity decreases nonlinearly with an increase in porosity. It has been well-established that there exists a nonlinear relation between the porosity of the fibrous medium and its permeability [53-57]. This is because, with the increase of porosity, the solid volume fraction decreases. Therefore, the fluid flows through less tortuous passes. Moreover, drag forces offered by the fibers decrease nonlinearly as the porosity increases. These in turn result in the nonlinear relation of permeability and porosity. Permeability is related to the flow resistivity as follows:

$$\sigma = \frac{\mu}{K} \tag{4}$$

where σ and K denote flow resistivity and permeability of fibrous medium and μ is viscosity.

According to Eq. 4, a nonlinear increase in permeability leads to a nonlinear decrease in flow resistivity.
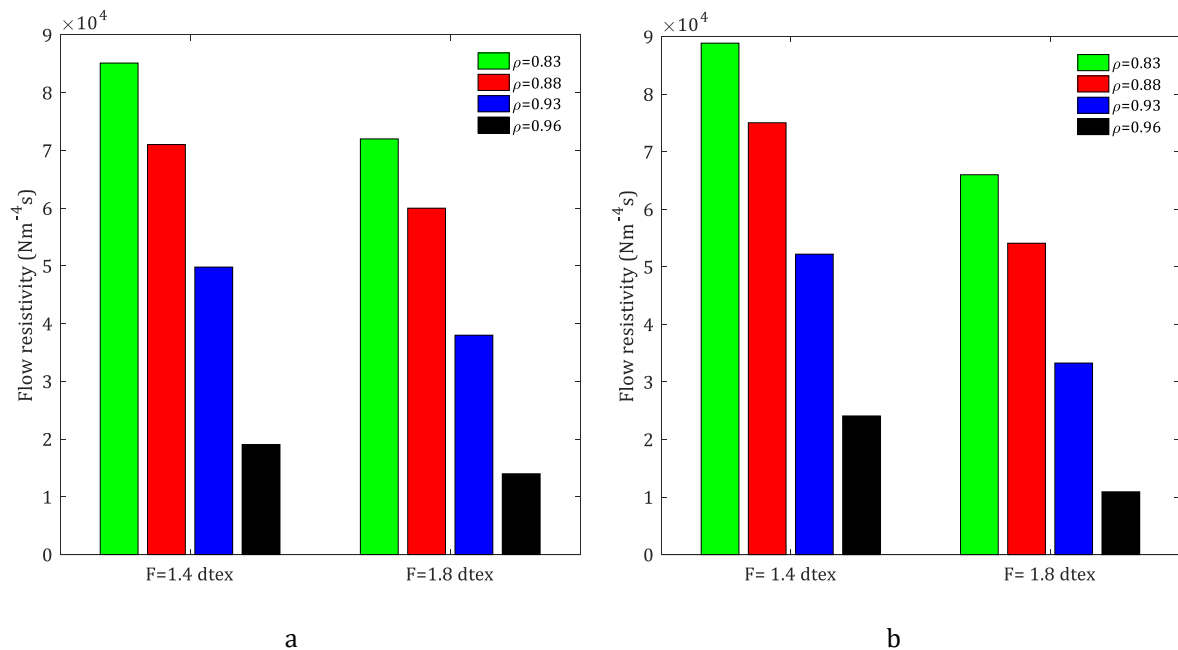
Fig. 4 Variations of flow resistivity vs. porosity and fiber linear density for samples with a thickness of a) 2 cm, and b) 3 cm

16

It is also noticed that flow resistivity decreases with the increase of fiber linear density. The unit of fiber linear density is dtex. It is defined as the weight, in grams, of 10000 meters of fiber. Therefore, a higher linear density indicates a coarser fiber. At the microscopic scale, the flow of fluid over the fibers results in the formation of a viscous boundary layer and consequently a resistance to the flow. An increase in fiber diameter under such a condition leads to a reduction in shearing of the boundary layer. Similar results were observed for the thickness of 3 cm (samples 9-16) and are shown in Fig. 4b.

The effects of TP orientation on flow resistivity are given in Table 1. In this Table, the orientation of fibers in the 3D space is shown using the diagonal components of the second-order orientation tensor a_{ij}. As previously mentioned, the diagonal components, i.e., a_{ii}, must always lie in the range [0, 1]. The tensor a is symmetric, and its trace always equals one, i.e., $a_{11} + a_{22} + a_{33} = 1$. The diagonal components serve to characterize the relative orientation in x-, y- and z-directions. Therefore, for an isotropic fibrous structure $a_{11} = a_{22} = a_{33} = 1/3$; for a fully layered fibrous structure $a_{11} = a_{22} = 1/2$, and $a_{33}=0$; and for a unidirectional structure with the orientation of fibers in the z-direction $a_{11} = a_{22} = 0$, and $a_{33}=1$. As observed in Table 1, for sample 21, fibers are orientated randomly in the fabric plane and partially oriented in z-direction. The almost similar values of a_{ii} for sample 1 indicates the isotropic orientation of fibers in the 3D space. In sample 22, fibers show random orientation in x- and y-directions, while they are moderately oriented in the z-direction. The a_{33} value for sample 23 (0.71) indicates the dominant orientation of fibers in z-direction.

As is observed, flow resistivity decreased with the increase of fiber orientation in the flow direction. This behavior is expected, as the drag forces are lower for flow parallel to the fibers. Additionally, with the increase of fiber orientation in the flow direction, the continuity of the voids through which the fluid flows increases, and consequently, flow

resistivity decreases. A similar trend was noticed for samples with a porosity of 0.93 (samples 24, 3, 25, and 26).

3.2 Sound absorption behavior

Variations of the SAC with frequency for samples with isotropic fiber orientation (samples 1-20) and different values of thickness, porosity, and fiber linear density are shown in Fig. 5. As is seen, for all samples the absorption mechanism belongs to the viscosity resistance type. In this mechanism, the SACs at low-frequency bands are very low, while at high frequencies are large. Referring to Fig. 5a, for the nonwovens with 2 cm thickness and fiber linear density of 1.4 dtex, samples 1 and 2 with low porosity values enjoy high absorption at frequencies below 1800 Hz, while they do not show good absorption at high-frequency bands. This is attributed to the fact that samples with low porosity values show high flow resistivities (85137 and 71021 $Nm^{-4}s$ for samples 1 and 2, respectively). Therefore, high-frequency sound cannot easily enter the porous structure of the sample, and hence absorption is weak [47].

Samples 1 and 2 have relatively the same SAC at frequencies below 1800 Hz. With the increase of porosity from 0.832 to 0.884, the SAC increases at high frequencies. The peak of absorption for samples 1 and 2 occurs at 3150 and 3500 Hz, respectively. With an increase in the porosity up to 0.933 (sample 3), the SAC slightly decreases at low frequencies and significantly increases at high-frequency bands. The peak of SAC for sample 3 occurs at 3500 Hz. Further increase in porosity decreases the SAC at both low and high frequencies (sample 4). These results indicate that for specimens with a thickness of 2 cm and fiber linear density of 1.4 dtex, the optimum porosity value to achieve the best sound absorption performance is 0.933. The result of the analysis of variance (ANOVA) showed that the porosity has a significant effect on the SAC (p-value < 0.05).

a) T= 2 cm, F= 1.4 dtex

b) T= 2 cm, F= 1.8 dtex

c) T= 3 cm, F= 1.4 dtex

d) T= 3 cm, F= 1.8 dtex

e) T= 4 cm, F= 1.4 dtex
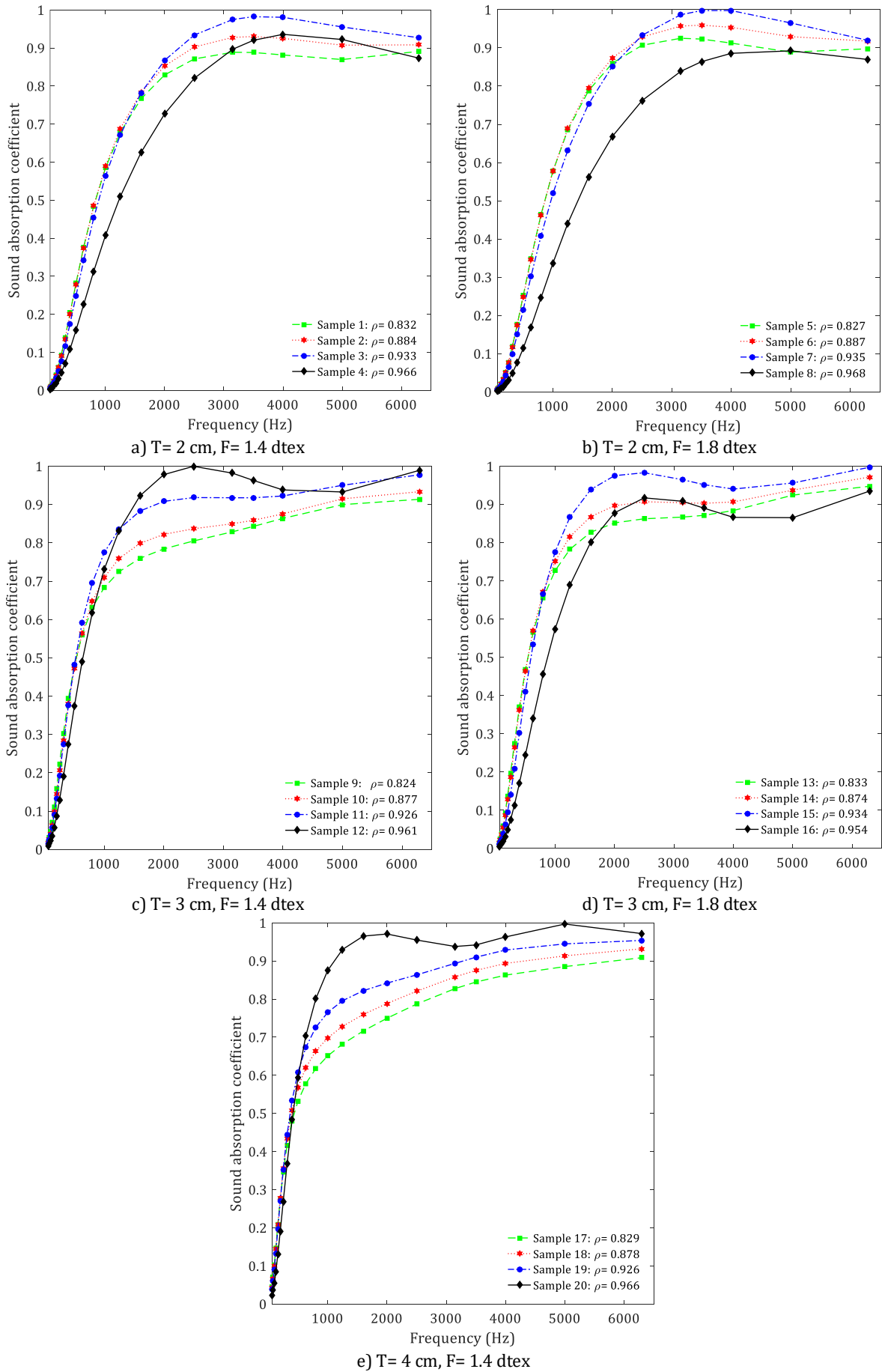
Fig. 5 SAC vs. frequency for samples with isotropic fiber orientation and different thickness, porosity, and fiber linear density values

19

Variations of the SAC with frequency for specimens with a thickness of 2 cm, fiber linear density of 1.8 dtex, and isotropic fiber orientation are shown in Fig. 5b. It is observed that similar to the samples made from 1.4 dtex fibers, the SAC increases with the increase of porosity up to 0.935, beyond which it experiences a significant decrease. It is also observed that for samples 5, 6, 7, and 8, the peak of SAC is 0.92, 0.96, 1, and 0.89 and respectively occurs at frequencies of 3150, 3500, 4000, and 5000 Hz.

Variations of the SAC with frequency for specimens with a thickness of 3 cm, fiber linear density of 1.4 dtex, and isotropic fiber orientation are shown in Fig. 5c. It is observed that the SAC in low-porosity samples (9 and 10) increases with an increase in the sound frequency, and no distinct peak is observed in the frequency range of 80-6300 Hz. With the increase of porosity from 0.877 to 0.926, the SAC decreases at frequencies below 315 Hz and rises at higher frequencies. A further increase in porosity leads to the remarkable improvement of the SAC at frequencies higher than 1250 Hz.

Fig. 5d depicts the variations of the SAC with frequency for samples with a thickness of 3 cm, fiber linear density of 1.8 dtex, and isotropic fiber orientation. It is noticed that the SAC improves with the increase of porosity up to 0.934, beyond which it reduces. It is seen that at frequencies above 800 Hz sample of 0.934 porosity demonstrates the best acoustic absorption performance.

Variations of the SAC with frequency for specimens with a thickness of 4 cm, fiber linear density of 1.4 dtex, and isotropic fiber orientation are shown in Fig. 5e. The results of the ANOVA test show that there is no significant difference between the SACs of the specimens at low frequencies. It is observed that the SAC increases with an increase in the porosity of the sample for frequencies above 400 Hz. For sample 20 with a porosity of 0.966, the SAC increases with the frequency up to 2000 Hz, beyond which it slightly reduces and then re-increases and reaches the SAC pack of 1 at 5000 Hz.

In order to further elucidate the effects of sample porosity and fiber linear density on the acoustic behavior of the samples, the frequency-dependent SAC curves of the samples at constant porosities are given in Fig. 6. As is observed in Fig. 6a, for samples 1 and 5 with a thickness of 2 cm and porosity of 0.83, the sample made of finer fibers (i.e., 1.4 dtex) enjoy higher absorption at low frequencies. This is attributed to the higher flow resistivity of sample 1 as compared with sample 5. However, at higher frequencies, samples made of coarser fibers (i.e., 1.8 dtex) provide higher sound absorption.
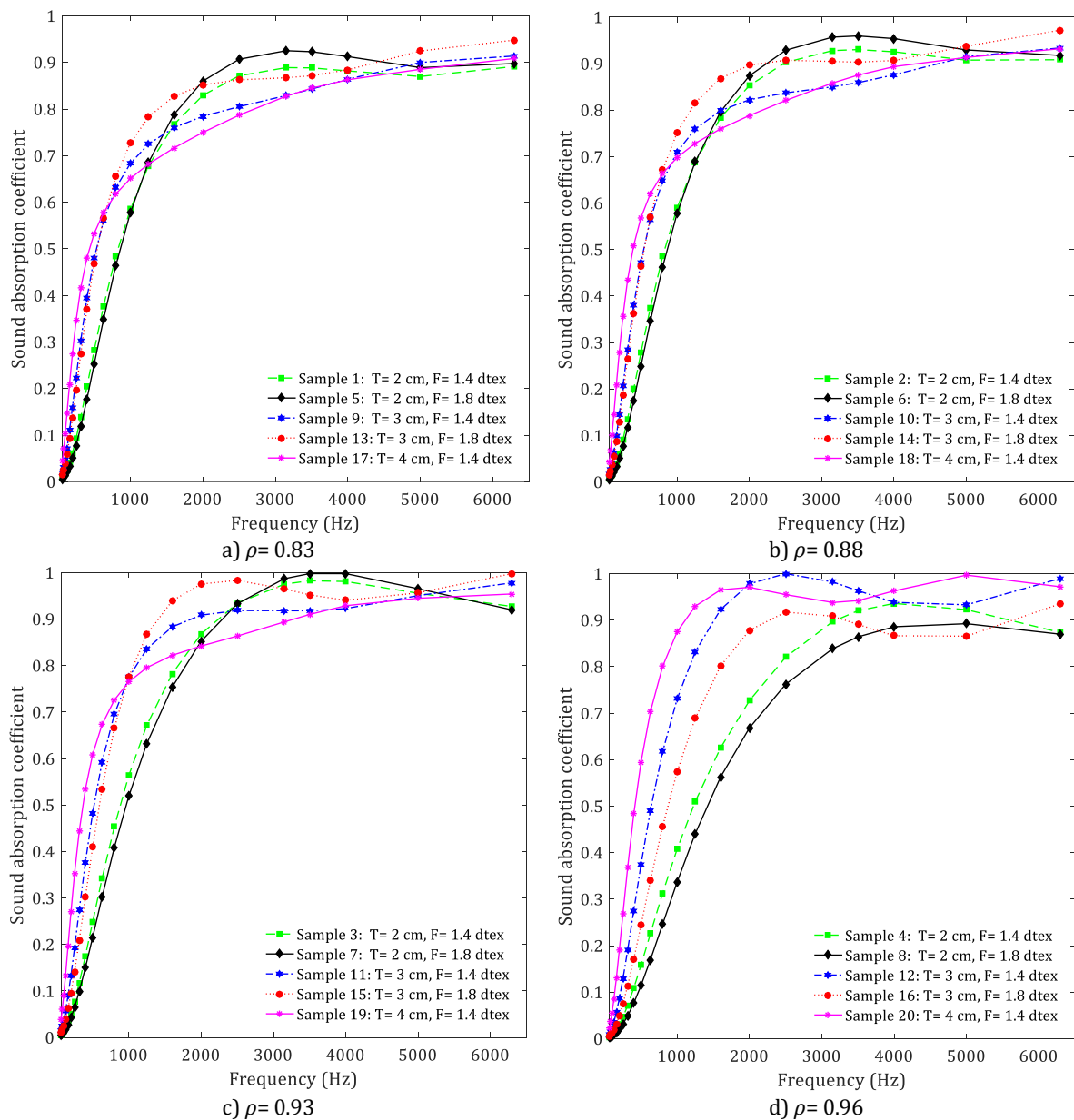
Fig. 6 SAC vs. frequency for samples with isotropic fiber orientation, different thicknesses, and fiber linear density values at constant porosities

21

Comparison of Fig. 6a with Figs. 6b and 6c shows that with the increase of sample porosity up to 0.93, the difference between the SACs of samples made of 1.4 and 1.8 dtex decreases. A further increase in porosity leads to higher absorption of finer fibers at higher frequencies (Fig. 6d). As is observed in this figure, samples made of finer fibers provide higher sound absorption for the low, mid, and high frequencies. These results show that high-porosity samples made of finer fibers provide excellent sound absorption performance.

Similar results are obtained for specimens with 3 cm thickness and isotropic fiber orientation. The results show that at all porosities, samples with a thickness of 4 cm provide higher absorption at low-frequency levels. It is concluded that in order to increase the SAC of nonwoven fabric at low-frequency ranges, it would be better to increase the thickness than to decrease the porosity. It is also concluded that increasing the thickness and fiber fineness results in the simultaneous improvement of the SAC at low-, mid-and high-frequency bands.

Fig. 7 depicts the effects of TP fiber orientation on the SAC of the samples at a thickness of 2 cm, fiber linear density of 1.4 dtex, and porosities of 0.83, 0.93, and 0.96. The results of the ANOVA test show that there is no significant difference between the SAC values of the low-porosity samples at frequencies below 2000 Hz (Fig. 7a). The SAA values for samples 21, 1, 22, and 23 are 0.449, 0.447, 0.443, and 0.438, respectively. These results show that TP fiber orientation does not affect the sound absorption behavior of low-porosity samples at low- and mid-frequency bands. However, at frequencies above 2000 Hz, sound absorption enhances with the increase of TP orientation. As shown in Fig. 7b, for samples with a porosity of 0.93, TP orientation does not significantly affect the SAC at frequencies below 400 Hz. However, at frequencies between 400-2000 Hz, samples with lower TP orientation demonstrate better acoustic absorption performance. The SAA

values for samples 24, 3, 25, and 26 are 0.464, 0.440, 0.425, and 0.389, respectively. At frequencies above 2000 Hz, samples with a higher degree of TP fiber orientation show better performance as the sound frequency increases. As shown in Fig. 7c, for samples with a porosity of 0.96, layered structures demonstrate superior acoustic behavior and the acoustic performance decreases with the increase of TP orientation. The SAA values for samples 27, 4, 28, and 29 are 0.421, 0.337, 0.324, and 0.273, respectively.
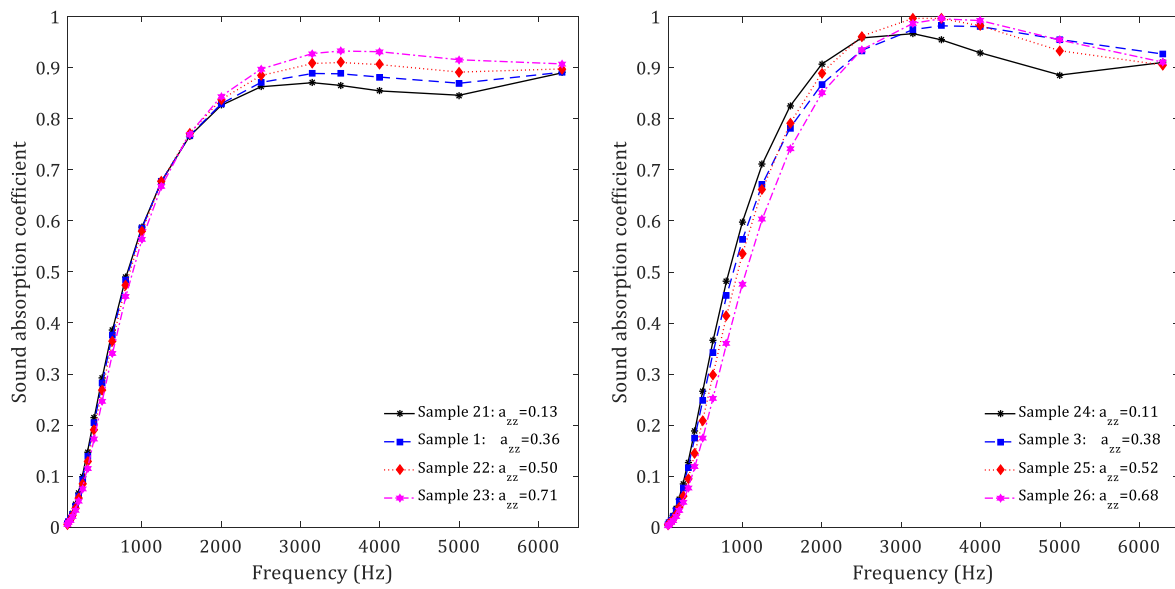
a) T= 2 cm, F= 1.4 dtex, ρ= 0.83

b) T= 2 cm, F= 1.4 dtex, ρ= 0.93
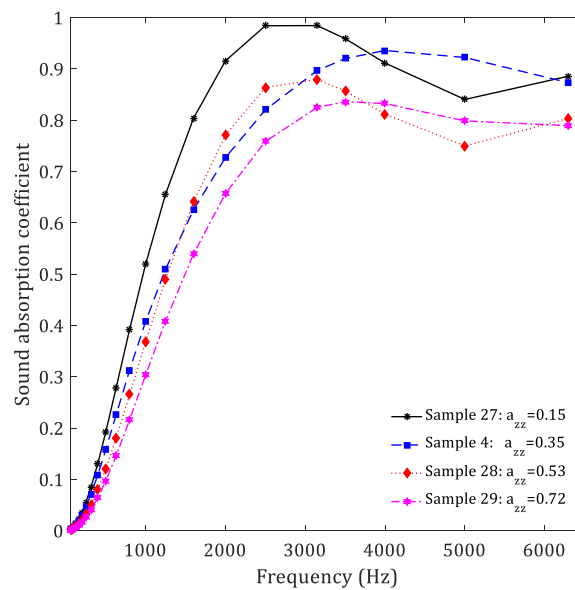
c) T= 2 cm, F= 1.4 dtex, ρ= 0.96

Fig. 7 Effect of through-plane fiber orientation on SAC

The effects of IP fiber orientation on the acoustic absorption characteristics of samples 24, 30, and 31 are shown in Fig. 8. As observed in Table 1, these samples are layered structures with the difference that, in sample 24 fibers are randomly orientated in the fabric plane ($x - y$ plane), while for sample 30 fibers are moderately oriented in x-direction, and for sample 31 fibers are dominantly oriented in the x-direction. The results show that at most frequencies, the IP orientation does not significantly affect the SAC, however at frequencies between 4000-6300 Hz, samples with random FOD in the fabric plane show relatively weaker absorption performance. It is worthy to mention that layered samples with dominant IP fiber orientation (samples 30 and 31) due to lower entanglement of fibers suffer from lower tensile strength and therefore, they cannot be a good candidate for practical applications. Comparison of Figs. 7 and 8 shows that TP fiber orientation has a more profound influence on the SAC of nonwoven fabrics as compared with the IP fiber orientation.
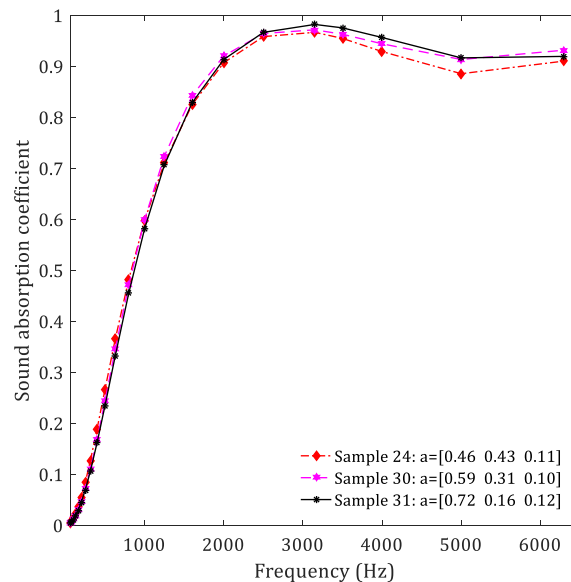
Fig. 8 Effect of in-plane fiber orientation on SAC

24

3.3 Thermal insulation properties

Fig. 9 shows the variation of K_{eff} with porosity and fiber fineness for specimens with a thickness of 2 cm. It is observed that K_{eff} significantly decreases with the increase of the porosity of nonwoven media. This is attributed to the fact that the thermal conductivity of air (0.0258 W.m^{-1}K^{-1} at 20°C) is much lower than that of PP fiber (0.101 W.m^{-1}K^{-1}). Additionally, it is observed that thicker fibers (1.8 dtex) lead to higher thermal conductivity values. At a given porosity, an increase in fiber diameter leads to a decrease in the number of fiber-to-fiber contacts. This, in turn, results in a reduction in the number of bottlenecks on the heat flow paths, thus the observed increase in the amount of heat transferred by conduction.
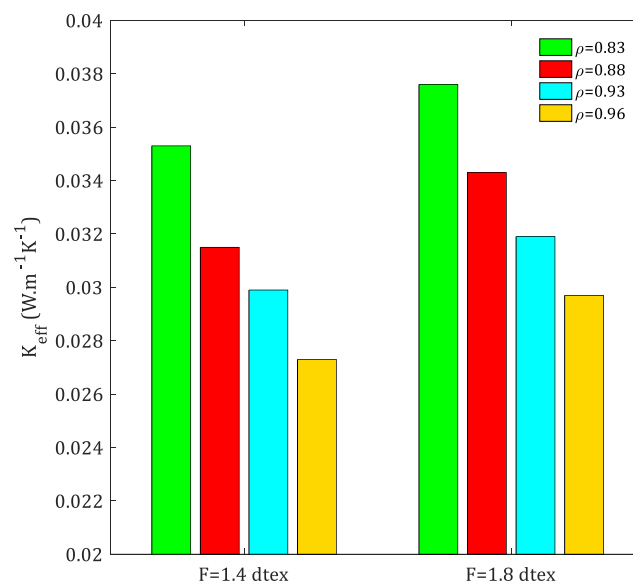
Fig. 9 Variations of effective thermal conductivity vs. porosity and fiber linear density for specimens with a thickness of 2 cm

Referring to Table 1, comparisons between the K_{eff} values for specimens of the same porosity, fiber fineness, and orientation show that fabric thickness does not significantly affect the effective thermal conductivity of samples, while it significantly affects the thermal resistance (samples 1-20).

Fig. 10 depicts how the TP fiber orientation affects K_{eff} for specimens with porosity of 0.83, 0.93, and 0.96. It is noticed that thermal conductivity increases with the increase of TP fiber orientation and this increase is more pronounced at lower porosities. In other words, K_{eff} raises with the increase of the proportion of fibers that are parallel to the heat flow direction. This is because an increase in TP fiber orientation increases the chance that heat flows along the length of the fibers as opposed to flowing in the direction perpendicular to fiber length where the fiber-to-fiber contact areas are considerably narrower [27]. Additionally, the thermal conductivity of fibers along their axis is in the range of 2-8 W.m^{-1}K^{-1}, while in the perpendicular direction is in the range of 0.1-0.55 W.m^{-1}K^{-1} [58]. For example, these values for PP fiber are 1.241 and 0.111 W.m^{-1}K^{-1}, respectively [25]. Thus it can be deduced that the heat flow rate is much larger when fibers are aligned parallel to heat flow direction. These results point to the significant influence of fiber anisotropy on the thermal insulation performance of nonwoven fabrics. The results of the statistical analysis also showed that IP fiber orientation does not significantly affect the K_{eff} of the samples.
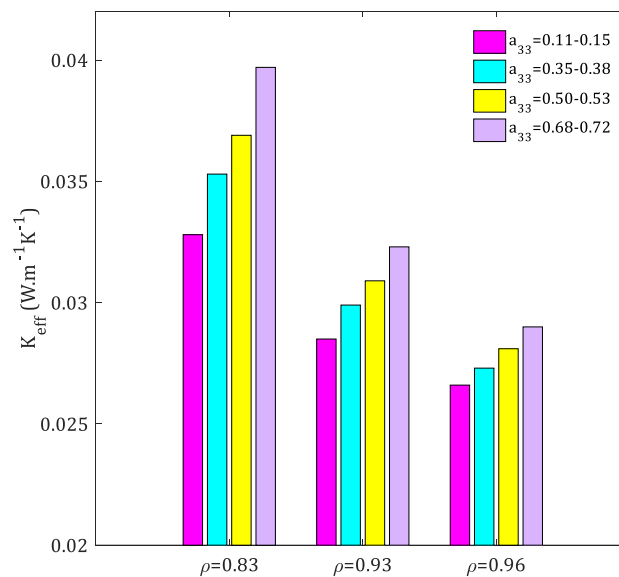
Fig. 10 Variations of effective thermal conductivity vs. through-plane fiber orientation and porosity

3.4 Comparison with some commercial products and literature data

As previously mentioned, a solution to achieve the highest possible thermal insulation and sound absorption performance in buildings is to increase the thickness of nonwoven media. However, thick insulations are not desirable for several reasons, including increased initial investment and material consumption, indoor floor space reductions, and architectural restrictions. In this section, for each thickness, samples with the highest SAA and lowest thermal conductivity were considered as the optimized samples and compared to some commercial counterparts, including polyurethane foam supplied from Mahar-Energy (Tehran, Iran); polyester nonwoven supplied from Mahoot Co. (Isfahan, Iran); needled glasswool purchased from Luyang energy-saving materials (Zibo, China); and wool felt fabric supplied from Pashmineh Co. (Isfahan, Iran). Hence, samples 24, 12, and 20 were chosen as the optimized samples for the thicknesses of 2, 3, and 4 cm, respectively, and their performances are compared with commercially available samples in Fig. 11.

In Fig. 11a, sample 24 (T= 2 cm, ρ= 0.928, F= 1.4 dtex) is compared with a polyurethane foam (T=2 cm, ρ= 0.922), needled polyester nonwoven (T= 2 cm, ρ= 0.935, F= 1.4 dtex), and needled glasswool (T= 2 cm, ρ= 0.926). It is observed that sample 24 enjoys the highest SAA. Additionally, its K_{eff} is lower than that of polyester nonwoven and glasswool. In Fig. 11b, sample 12 (T= 3 cm, ρ= 0.961, F= 1.4 dtex) is compared with a needled polyester nonwoven (T= 3 cm, ρ= 0.951, F= 1.3 dtex), and needled glasswool (T= 3 cm, ρ= 0.957). The results show that, sample 22 shows the best sound absorption and very good thermal insulation performance. Comparison of sample 20 (T= 4 cm, ρ= 0.966, F= 1.4 dtex) with a needled polyester nonwoven (T= 4 cm, ρ= 0.958, F= 1.4 dtex), needled glasswool (T= 4 cm, ρ= 0.963), and wool felt fabric (T= 4 cm, ρ= 0.951, F= 3.2 dtex) is shown in Fig. 11c. It is observed that sample 20 has the highest SAA and its K_{eff} is lower

than those of polyester nonwoven and wool felt fabric. These results point to the promising acoustic absorption and thermal insulation properties of polypropylene nonwoven fabrics. It is worthy to mention that PP nonwovens have a comparable price to conventional building insulation materials. Additionally, for the application of building insulation, PP nonwovens can be produced from the recycled and waste PP fibers that are globally abundant.

a) T= 2 cm

b) T= 3 cm

c) T= 4 cm
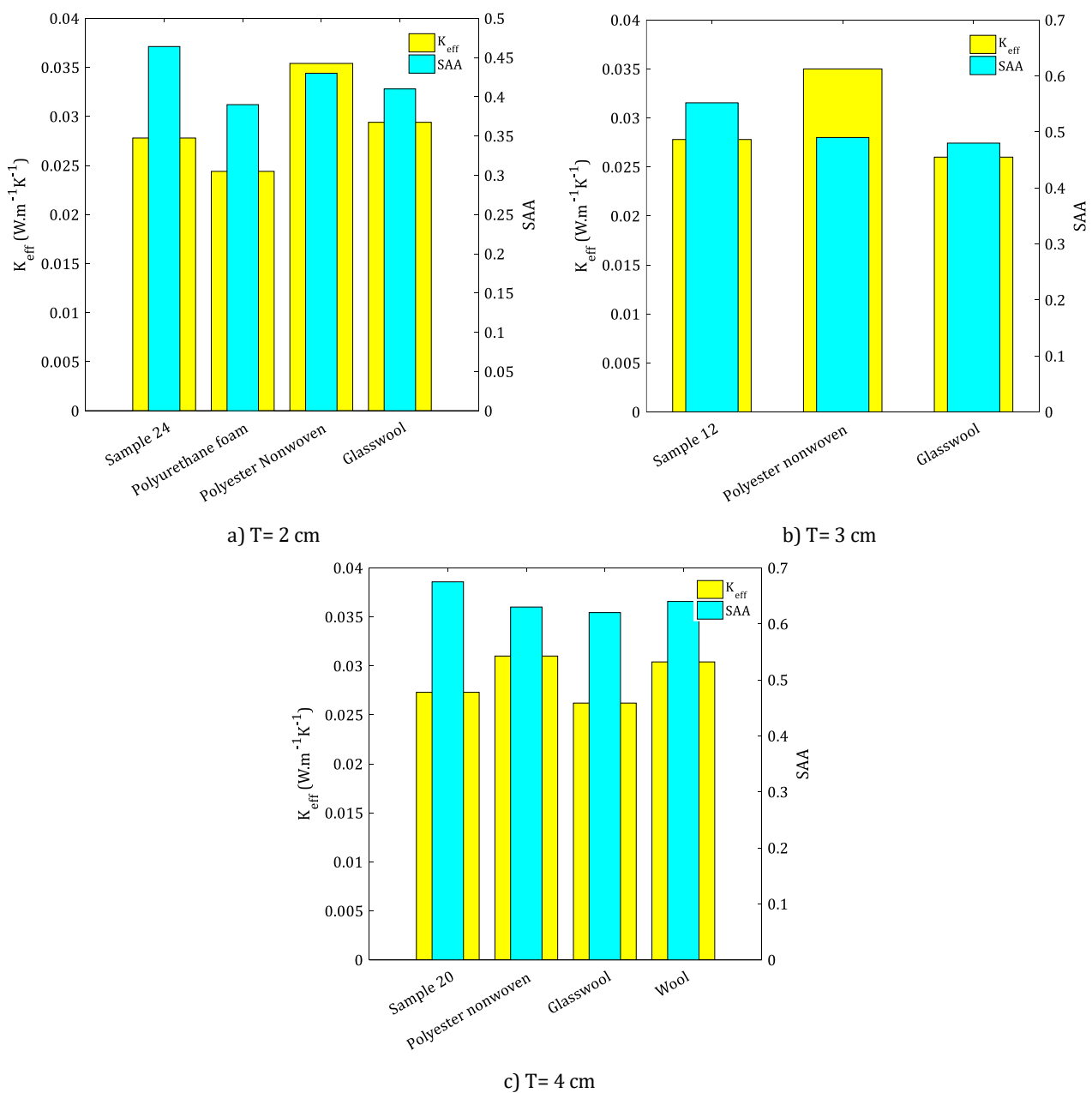
Fig. 11 The SAA and K_{eff} values for the optimized samples and comparison with some commercial products

The SAA and K_{eff} values of some of the samples were also compared with some literature data and are given in Tables 2 and 3, respectively. As is observed, the SAA and K_{eff} of the optimal specimens could be engineered in the ranges of 0.43-0.60, and 0.0274-0.0301 W.m^{-1}K^{-1}, respectively, suggesting that PP nonwovens enjoy promising acoustic and thermal performance compared with fibrous and foamed materials of the same thickness and density.

Table 2 Comparison of the SAA values of the samples with some literature data

Thickness (cm)	Bulk density (kg/m³)	Sound absorber material	SAA	Reference
2	100	Sample 2	0.43	Current work
		Date palm	0.38	[35]
		Phenolic resin-bonded recycled denim	0.37	[32]
		kenaf fibers/rice husk composite	0.39	[59]
2	150	Sample 1	0.44	Current work
		Phenolic resin-bonded recycled denim	0.38	[32]
		Flax fiber-reinforced polypropylene composite	0.31	[60]
3	100	Sample 10	0.55	Current work
		Date palm	0.43	[35]
		Kenaf fibers/rice husk composite	0.50	[59]
		Nut leaf sheath fibers	0.52	[61]
		Recycled surgical face mask	0.58	[62]
		Cork	0.44	[40]
3	150	Sample 13	0.56	Current work
		Kenaf	0.50	[39]
		Recycled surgical face mask	0.56	[62]
		Chrome shave and coffee silver skin	0.51	[63]
4	100	Sample 18	0.60	Current work
		Date palm	0.58	[35]
		Kenaf fibers/rice husk composite	0.65	[59]
		Nut leaf sheath fibers	0.51	[61]
4	150	Sample 17	0.57	Current work
		Kenaf	0.53	[39]

Table 3 Comparison of the K_{eff} values of the samples with some literature data

Thickness (cm)	Bulk density (kg/m³)	Thermal insulation material	K_{eff}	Reference
2	30	Sample 4	0.0274	Current work
		100% wool	0.0400	[64]
		Sheep wool	0.0341	[65]
		Flax	0.0390	[66]
		Polyurethane foam	0.024	[67]
		Extruded polystyrene	0.0300	[67]
2	60	Sample 3	0.0299	Current work
		Recycled polyester	0.0340	[15]
		Waste wool and recycled polyester	0.0320	[15]
		Fiber glass	0.0330	[67]
		Hemp and cellulose fibers	0.0460	[68]
		Hollow microspheres	0.0390	[69]
2	100	Sample 2	0.0315	Current work
		Kenaf and Polyester blend	0.0400	[64]
		Fiberglass	0.0320	[67]
		Jute	0.0380	[70]
3	30	Sample 12	0.0278	Current work
		Wood	0.0460	[67]
		Hemp and cellulose fibers	0.0460	[68]
		Carpet waste wool	0.0301	[71]
3	60	Sample 11	0.0301	Current work
		Recycled polyester	0.0340	[15]
		Polyurethane foam	0.0220	[67]
		Fiberglass	0.0330	[67]
		Phenolic foam	0.0260	[70]
4	30	Sample 20	0.0277	Current work
		Sheep wool	0.0320	[65]
		Polyurethane foam	0.0200	[67]
		Hemp and cellulose fibers	0.0440	[68]

4. Conclusion

Thermal insulation and acoustic absorption materials are critical to reducing energy consumption and noise pollution in buildings, however, these two types of materials are generally developed independently. This study investigated the acoustic and heat transfer properties of lightweight needled nonwoven fabrics for building applications. Nonwoven fabrics with different structural properties were produced and the effects of structural properties on thermal insulation and sound absorption performance were investigated. The K_{eff} and SAA of the samples could be engineered in the 0.0270-0.0404 W.m^{-1}K^{-1} and 0.270–0.675 ranges, respectively. It was found that fiber fineness has a profound effect on acoustic absorption and thermal insulation properties. Samples made of finer fibers enjoyed higher sound absorption and thermal resistance. It was shown that IP orientation has not a significant effect on sound absorption and thermal insulation. An increase in TP fiber orientation negatively affected the thermal insulation properties, while its effect on acoustic behavior depends on the porosity of samples and the sound wave frequency. Generally, an increase in TP orientation adversely affects the acoustic characteristics of high porosity samples, while it enhances the acoustic behavior of samples with low porosity. The best acoustic and thermal performance were achieved by fibrous samples of layered structure made of 1.4 dtex fibers with a thickness of 3 cm (SAA= 0.552, K_{eff}=0.0278 W.m^{-1}K^{-1}) and 4 cm (SAA= 0.675, K_{eff}=0.0277 W.m^{-1}K^{-1}). PP nonwoven fabrics, therefore, have great potential as candidate materials for building applications due to excellent chemical and corrosion resistance, very low moisture absorption, low density, and the ability to engineer the thermal and acoustical properties.

These fibrous structures can be placed on walls or ceilings to control and reduce noise and heat transmission. These fibrous structures can also be used as a cover for rigid

surfaces and walls in applications such as interior finishing in buildings that aesthetically and artistically pleasing appearance is important.

It is worthy to mention that the potential for flammability may limit the usage of PP fibers in construction and renovation projects. Flame retardant properties can significantly be improved via a facile treatment with flame retardant finishes and coatings or incorporation of flame retardant additives into polymer melt in the melt-spinning process while maintaining the sound absorption and thermal insulation properties.

Funding

References

[1] M. Kenisarin, K. Mahkamov, Passive thermal control in residential buildings using phase change materials, Renewable and Sustainable Energy Reviews 55 (2016) 371-398.

[2] N.A. Khan, B. Bhattacharjee, Thermal and noise insulation performance interaction of building envelope during building simulation optimization in tropical climates, Building and Environment (2021) 107948.

[3] C. Nägeli, C. Camarasa, M. Jakob, G. Catenazzi, Y. Ostermeyer, Synthetic building stocks as a way to assess the energy demand and greenhouse gas emissions of national building stocks, Energy and Buildings 173 (2018) 443-460.

[4] K. Valančius, T. Vilutienė, A. Rogoža, Analysis of the payback of primary energy and CO_2 emissions in relation to the increase of thermal resistance of a building, Energy and Buildings 179 (2018) 39-48.

[5] A. Hadded, S. Benltoufa, F. Fayala, A. Jemni, Thermophysical characterization of recycled textile materials used for building insulating, Journal of Building Engineering 5 (2016) 34-40.

[6] E. Latif, S. Tucker, M.A. Ciupala, D.C. Wijeyesekera, D.J. Newport, M. Pruteanu, Quasi steady-state and dynamic hygrothermal performance of fibrous Hemp and Stone Wool insulations: Two innovative laboratory-based investigations, Building and Environment 95 (2016) 391-404.

[7] N.M. Aly, H. Seddeq, K. Elnagar, T. Hamouda, Acoustic and thermal performance of sustainable fiber reinforced thermoplastic composite panels for insulation in buildings, Journal of Building Engineering (2021) 102747.

[8] H. Gao, H. Liu, L. Liao, L. Mei, G. Lv, L. Liang, G. Zhu, Z. Wang, D. Huang, Improvement of performance of foam perlite thermal insulation material by the design of a triple-hierarchical porous structure, Energy and Buildings 200 (2019) 21-30.

[9] M. Ibrahim, K. Nocentini, M. Stipetic, S. Dantz, F.G. Caiazzo, H. Sayegh, L. Bianco, Multi-field and multi-scale characterization of novel super insulating panels/systems based on silica aerogels: Thermal, hydric, mechanical, acoustic, and fire performance, Building and Environment 151 (2019) 30-42.

[10] S. Fantucci, S. Garbaccio, A. Lorenzati, M. Perino, Thermo-economic analysis of building energy retrofits using VIP-Vacuum Insulation Panels, Energy and Buildings 196 (2019) 269-279.

[11] A.W.A. Hammad, A. Akbarnezhad, P. Oldfield, Optimising embodied carbon and U-value in load bearing walls: A mathematical bi-objective mixed integer programming approach, Energy and Buildings 174 (2018) 657-671.

[12] B. Abu-Jdayil, A.-H. Mourad, W. Hittini, M. Hassan, S. Hameedi, Traditional, state-of-the-art and renewable thermal building insulation materials: An overview, Construction and Building Materials 214 (2019) 709-735.

[13] B.P. Jelle, Traditional, state-of-the-art and future thermal building insulation materials and solutions–Properties, requirements and possibilities, Energy and Buildings 43(10) (2017) 2549-2563.

[14] A. Fahimifar, A. Abdolmaleki, P. Soltani, Stabilization of rock slopes using geogrid boxes, Arabian Journal of Geosciences 7(2) (2014) 609-621.

[15] A. Patnaik, M. Mvubu, S. Muniyasamy, A. Botha, R.D. Anandjiwala, Thermal and sound insulation materials from waste wool and recycled polyester fibers and their biodegradation studies, Energy and Buildings 92 (2015) 161-169.

[16] R. Muthuraj, C. Lacoste, P. Lacroix, A. Bergeret, Sustainable thermal insulation biocomposites from rice husk, wheat husk, wood fibers and textile waste fibers: Elaboration and performances evaluation, Industrial Crops and Products 135 (2019) 238-245.

[17] N. Nazeran, J. Moghaddas, Synthesis and characterization of silica aerogel reinforced rigid polyurethane foam for thermal insulation application, Journal of Non-Crystalline Solids 461 (2017) 1-11.

[18] F. Wang, Z. Chen, C. Wu, Modeling and estimation of thermal conductivity of ultrafine glass wool mats by artificial neural network and correlation, The Journal of the Textile Institute 110(11) (2019) 1562-1568.

[19] K. Miskinis, V. Dikavicius, A. Buska, K. Banionis, Influence of EPS, mineral wool and plaster layers on sound and thermal insulation of a wall: a case study, Applied Acoustics 137 (2018) 62-68.

[20] M.M. Seraji, S. Kianersi, S.H. Hosseini, J. Davarpanah, S. Elahi, Performance evaluation of glass and rock wool fibers to improve thermal stability and mechanical strength of monolithic phenol-formaldehyde based carbon aerogels, Journal of Non-Crystalline Solids 491 (2018) 89-97.

[21] H. Gao, L. Liao, H. Liu, L. Mei, Z. Wang, D. Huang, G. Lv, G. Zhu, C. Wang, Optimization of thermal insulation performance of porous geopolymers under the guidance of thermal conductivity calculation, Ceramics International Available online (2020).

[22] Y.K. Godovsky, Thermophysical Properties of Polymers, Springer Science & Business Media2012.

[23] C. Bai, P. Colombo, Processing, properties and applications of highly porous geopolymers: A review, Ceramics International 44(14) (2018) 16103-16118.

[24] A. Patti, A. Domenico, Thermal Conductivity of Polypropylene-Based Materials, Polypropylene, IntechOpen2019.

[25] M.O.R. Siddiqui, D. Sun, I.B. Butler, Geometrical modelling and thermal analysis of nonwoven fabrics, Journal of Industrial Textiles 48(2) (2018) 405-431.

[26] M. Tahir, H.V. Tafreshi, S. Hosseini, B. Pourdeyhimi, Modeling the role of microstructural parameters in radiative heat transfer through disordered fibrous media, International Journal of Heat and Mass Transfer 53(21-22) (2010) 4629-4637.

[27] R. Arambakam, H.V. Tafreshi, B. Pourdeyhimi, Modeling performance of multi-component fibrous insulations against conductive and radiative heat transfer, International Journal of Heat and Mass Transfer 71 (2014) 341-348.

[28] P. Kaleeswaran, V.K. Kothari, Thermal resistance of nonwoven waddings, The Journal of the Textile Institute 108(10) (2017) 1657-1661.

[29] I. Cerkez, H.B. Kocer, R.M. Broughton, Airlaid nonwoven panels for use as structural thermal insulation, The Journal of the Textile Institute 109(1) (2018) 17-23.

[30] Z.M. Ghermezgoli, M. Moezzi, J. Yekrang, S.A. Rafat, P. Soltani, F. Barez, Sound absorption and thermal insulation characteristics of fabrics made of pure and crossbred sheep waste wool, Journal of Building Engineering 35 (2021) 102060.

[31] E. Taban, S. Amininasab, U. Berardi, D.D. Abdi, S.E. Samaei, Use of date palm waste fibers as sound absorption material, Journal of Building Engineering (2021) 102752.

[32] P. Hassani, P. Soltani, M. Ghane, M. Zarrebini, Porous resin-bonded recycled denim composite as an efficient sound-absorbing material, Applied Acoustics 173 (2021) 107710.

[33] F. D'Alessandro, F. Asdrubali, N. Mencarelli, Experimental evaluation and modelling of the sound absorption properties of plants for indoor acoustic applications, Building and Environment 94 (2015) 913-923.

[34] R. Abedkarimi, H. Hasani, P. Soltani, Z. Talebi, Experimental and computational analysis of acoustic characteristics of warp-knitted spacer fabrics, The Journal of The Textile Institute 111(4) (2020) 491-498.

[35] E. Taban, A. Khavanin, A. Ohadi, A. Putra, A.J. Jafari, M. Faridan, A. Soleimanian, Study on the acoustic characteristics of natural date palm fibres: Experimental and theoretical approaches, Building and Environment 161 (2019) 106274.

[36] H. Palak, B.K. Kayaoğlu, Analysis of the effect of fiber cross-section and different bonding methods on sound absorption performance of PET fiber-based nonwovens using Taguchi method, The Journal of the Textile Institute 111(4) (2020) 575-585.

[37] F. Suvari, Y. Ulcay, B. Maze, B. Pourdeyhimi, Acoustical absorptive properties of spunbonded nonwovens made from islands-in-the-sea bicomponent filaments, The Journal of the Textile Institute 104(4) (2013) 438-445.

[38] F. Shahani, P. Soltani, M. Zarrebini, The analysis of acoustic characteristics and sound absorption coefficient of needle punched nonwoven fabrics, Journal of Engineered Fibers and Fabrics 9(2) (2014) 84-92.

[39] E. Taban, P. Soltani, U. Berardi, A. Putra, S.M. Mousavi, M. Faridan, S.E. Samaei, A. Khavanin, Measurement, modeling, and optimization of sound absorption performance of Kenaf fibers for building applications, Building and Environment 180 (2020) 107087.

[40] U. Berardi, G. Iannace, Acoustic characterization of natural fibers for sound absorption applications, Building and Environment 94 (2015) 840-852.

[41] S. Mehrzad, E. Taban, P. Soltani, S.E. Samaei, A. Khavanin, Sugarcane bagasse waste fibers as novel thermal insulation and sound-absorbing materials for application in sustainable buildings, Building and Environment 211 (2022) 108753.

[42] C. Othmani, M. Taktak, A. Zein, T. Hentati, T. Elnady, T. Fakhfakh, M. Haddar, Experimental and theoretical investigation of the acoustic performance of sugarcane wastes based material, Applied Acoustics 109 (2016) 90-96.

[43] M.A. Biot, Theory of propagation of elastic waves in a fluid-saturated porous solid: II. Higher frequency range, J. Acoust. Soc. Am. 28(2) (1956) 179-191.

[44] U. Berardi, G. Iannace, Predicting the sound absorption of natural materials: Best-fit inverse laws for the acoustic impedance and the propagation constant, Applied Acoustics 115 (2017) 131-138.

[45] E. Taban, F. Valipour, D. Abdi, S. Amininasab, Mathematical and experimental investigation of sound absorption behavior of sustainable kenaf fiber at low frequency, International Journal of Environmental Science Technology 18(9) (2021) 2765-2780.

[46] P. Soltani, M. Azimian, A. Wiegmann, M. Zarrebini, Experimental and computational analysis of sound absorption behavior in needled nonwovens, J. Sound Vib. 426 (2018) 1-18.

[47] P. Soltani, M. Norouzi, Prediction of the sound absorption behavior of nonwoven fabrics: Computational study and experimental validation, Journal of Sound and Vibration 485 (2020) 115607.

[48] H.T. Luu, C. Perrot, R. Panneton, Influence of porosity, fiber radius and fiber orientation on the transport and acoustic properties of random fiber structures, Acta Acustica united with Acustica 103(6) (2017) 1050-1063.

[49] N. Kino, T. Ueno, Investigation of sample size effects in impedance tube measurements, Applied Acoustics 68(11-12) (2007) 1485-1493.

[50] G.W. Zack, W.E. Rogers, S.A. Latt, Automatic measurement of sister chromatid exchange frequency, Journal of Histochemistry and Cytochemistry 25(7) (1977) 741-753.

[51] J. Viguié, P. Latil, L. Orgéas, P. Dumont, S.R. du Roscoat, J.-F. Bloch, C. Marulier, O. Guiraud, Finding fibres and their contacts within 3D images of disordered fibrous media, Composites Science and Technology 89 (2013) 202-210.

[52] P. Soltani, M.S. Johari, M. Zarrebini, 3D fiber orientation characterization of nonwoven fabrics using X-ray micro-computed tomography, World Journal of Textile Engineering and Technology 1(0) (2015) 41-7.

[53] P. Soltani, M.S. Johari, M. Zarrebini, Effect of 3D fiber orientation on permeability of realistic fibrous porous networks, Powder Technology 254 (2014) 44-56.

[54] A. Nabovati, E.W. Llewellin, A.C. Sousa, A general model for the permeability of fibrous porous media based on fluid flow simulations using the lattice Boltzmann method, Composites Part A: Applied Science and Manufacturing 40(6-7) (2009) 860-869.

[55] M.M. Tomadakis, T.J. Robertson, Viscous permeability of random fiber structures: comparison of electrical and diffusional estimates with experimental and analytical results, Journal of Composite Materials 39(2) (2005) 163-188.

[56] P. Soltani, M. Zarrebini, R. Laghaei, A. Hassanpour, Prediction of permeability of realistic and virtual layered nonwovens using combined application of X-ray μCT and computer simulation, Chemical Engineering Research and Design 124 (2017) 299-312.

[57] S. Jaganathan, H.V. Tafreshi, B. Pourdeyhimi, A realistic approach for modeling permeability of fibrous media: 3-D imaging coupled with CFD simulation, Chemical Engineering Science 63(1) (2008) 244-252.

[58] S. Kawabata, Measurement of anisotropic thermal conductivity of single fiber, Journal of the Textile Machinery Society of Japan 39(12) (1986) T184-T186.

[59] S.E. Samaei, U. Berardi, E. Taban, P. Soltani, S.M. Mousavi, Natural fibro-granular composite as a novel sustainable sound-absorbing material, Applied Acoustics 181 (2021) 108157.

[60] K. Huang, U. Kureemun, W.S. Teo, H.P. Lee, Vibroacoustic behavior and noise control of flax fiber-reinforced polypropylene composites, Journal of Natural Fibers 16(5) (2019) 729-743.

[61] M. Raj, S. Fatima, N. Tandon, A study of areca nut leaf sheath fibers as a green sound-absorbing material, Applied Acoustics 169 (2020) 107490.

[62] R. Maderuelo-Sanz, P. Acedo-Fuentes, F.J. García-Cobos, F.J. Sánchez-Delgado, M.I. Mota-López, J.M. Meneses-Rodríguez, The recycling of surgical face masks as sound porous absorbers: Preliminary evaluation, Science of The Total Environment 786 (2021) 147461.

[63] D.D. Abdi, M. Monazzam, E. Taban, A. Putra, F. Golbabaei, M. Khadem, Sound absorption performance of natural fiber composite from chrome shave and coffee silver skin, Applied Acoustics 182 (2021) 108264.

[64] R. Pennacchio, L. Savio, D. Bosia, F. Thiebat, G. Piccablotto, A. Patrucco, S. Fantucci, Fitness: Sheep-wool and hemp sustainable insulation panels, Energy Procedia 111 (2017) 287-297.

[65] J. Zach, A. Korjenic, V. Petránek, J. Hroudová, T. Bednar, Performance evaluation and research of alternative thermal insulations based on sheep wool, Energy and Buildings 49 (2012) 246-253.

[66] A. Korjenic, V. Petránek, J. Zach, J. Hroudová, Development and performance evaluation of natural thermal-insulation materials composed of renewable resources, Energy and Buildings 43(9) (2011) 2518-2523.

[67] M.S. Al-Homoud, Performance characteristics and practical applications of common building thermal insulation materials, Building and Environment 40(3) (2005) 353-366.

[68] M. Reif, J. Zach, J. Hroudová, Studying the properties of particulate insulating materials on natural basis, Procedia Engineering 151 (2016) 368-374.

[69] X. Ji, H. Zhang, Z. Bai, G. Qiu, M. Guo, F. Cheng, M. Zhang, Self-assembled multifunctional bulk hollow microspheres: Thermal insulation, sound absorption and fire resistance, Energy and Buildings 205 (2019) 109533.

[70] S. Schiavoni, F. Bianchi, F. Asdrubali, Insulation materials for the building sector: A review and comparative analysis, Renewable and Sustainable Energy Reviews 62 (2016) 988-1011.

[71] M. El Wazna, M. El Fatihi, A. El Bouari, O. Cherkaoui, Thermophysical characterization of sustainable insulation materials made from textile waste, journal of Building Engineering 12 (2017) 196-201.